
LEARNING UNSIGNED DISTANCE FIELDS FROM LOCAL SHAPE FUNCTIONS FOR 3D SURFACE RECONSTRUCTION

A PREPRINT

Jiangbei Hu^{†*}
Dalian University of Technology
China

Yanggeng Li[†]
Nanyang Technological University
Singapore

Fei Hou
Chinese Academy of Sciences
China

Junhui Hou
City University of Hong Kong

Zhebin Zhang
InnoPeak Technology

Shengfa Wang
Dalian University of Technology
China

Na Lei
Dalian University of Technology
China

Ying He[‡]
Nanyang Technological University
Singapore

July 2, 2024

ABSTRACT

Unsigned distance fields (UDFs) provide a versatile framework for representing a diverse array of 3D shapes, encompassing both watertight and non-watertight geometries. Traditional UDF learning methods typically require extensive training on large datasets of 3D shapes, which is costly and often necessitates hyperparameter adjustments for new datasets. This paper presents a novel neural framework, *LoSF-UDF*, for reconstructing surfaces from 3D point clouds by leveraging local shape functions to learn UDFs. We observe that 3D shapes manifest simple patterns within localized areas, prompting us to create a training dataset of point cloud patches characterized by mathematical functions that represent a continuum from smooth surfaces to sharp edges and corners. Our approach learns features within a specific radius around each query point and utilizes an attention mechanism to focus on the crucial features for UDF estimation. This method enables efficient and robust surface reconstruction from point clouds without the need for shape-specific training. Additionally, our method exhibits enhanced resilience to noise and outliers in point clouds compared to existing methods. We present comprehensive experiments and comparisons across various datasets, including synthetic and real-scanned point clouds, to validate our method’s efficacy.

1 Introduction

3D surface reconstruction from raw point clouds is a significant and long-standing problem in computer graphics and machine vision. Traditional techniques like Poisson Surface Reconstruction[1] create an implicit indicator function from oriented points and reconstruct the surface by extracting an appropriate isosurface. The advancement of artificial intelligence has led to the emergence of numerous neural network-based methods for 3D reconstruction. Among these, neural implicit representations have gained significant influence, which utilize signed distance fields (SDFs) [2, 3, 4, 5, 6, 7, 8] and occupancy fields [9, 10, 11, 12] to implicitly depict 3D geometries. SDFs and occupancy fields extract isosurfaces by solving regression and classification problems, respectively. However, both techniques require internal and external definitions of the surfaces, limiting their capability to reconstructing only watertight geometries.

*Part of the project was completed when J. Hu was a Research Fellow at NTU.

[†]J. Hu and Y. Li contribute equally to the project.

[‡]Corresponding author: Y. He (yhe@ntu.edu.sg)

Therefore, unsigned distance fields [13, 14, 15, 16, 17, 18, 19, 20] have recently gained increasing attention due to their ability to reconstruct non-watertight surfaces and complex geometries with arbitrary topologies.

Reconstructing 3D geometries from raw point clouds using UDFs presents significant challenges due to the non-differentiability near the surface. This characteristic complicates the development of loss functions and undermines the stability of neural network training. Various unsupervised approaches [17, 14, 19] have been developed to tailor loss functions that leverage the intrinsic characteristics of UDFs, ensuring that the reconstructed geometry aligns closely with the original point clouds. However, these methods suffer from slow convergence, necessitating an extensive network training time to reconstruct a single geometry. As a supervised method, GeoUDF [15] learns local geometric priors through training on datasets such as ShapeNet [21], thus achieving efficient UDF estimation. Nonetheless, the generalizability of this approach is dependent on the training dataset, which also leads to relatively high computational costs.

In this paper, we propose a lightweight and effective supervised learning framework, *Losf-UDF*, to address these challenges. Since learning UDFs does not require determining whether a query point is inside or outside the geometry, it is a local quantity independent of the global context. Inspired by the observation that 3D shapes manifest simple patterns within localized areas, we synthesize a training dataset comprising a set of point cloud patches by utilizing local shape functions. Subsequently, we can estimate the unsigned distance values by learning local geometric features through an attention-based network. Our approach distinguishes itself from existing methods by its novel training strategy. Specifically, it is uniquely trained on synthetic surfaces, yet it demonstrates remarkable capability in predicting UDFs for a wide range of common surface types. For smooth surfaces, we generate training patches (quadratic surfaces) by analyzing principal curvatures, meanwhile, we design simple shape functions to simulate sharp features. This strategy has three unique advantages. First, it systematically captures the local geometries of most common surfaces encountered during testing, effectively mitigating the dataset dependence risk that plagues current UDF learning methods. Second, for each training patch, the ground-truth UDF is readily available, streamlining the training process. Third, this approach substantially reduces the costs associated with preparing the training datasets. We evaluate our framework on various datasets and demonstrates its ability to robustly reconstruct high-quality surfaces, even for point clouds with noise and outliers. Notably, our method can serve as a lightweight initialization that can be integrated with existing unsupervised methods to enhance their performance. We summarize our main contributions as follows.

- We present a simple yet effective data-driven approach that learns UDFs directly from a synthetic dataset consisting of point cloud patches, which is independent of the global shape.
- Our method is computationally efficient and requires training only once on our synthetic dataset. Then it can be applied to reconstruct a wide range of surface types.
- Our framework achieves superior performance in surface reconstruction from both synthetic point clouds and real scans, even in the presence of noise and outliers.

2 Related Work

Surface reconstruction. Reconstructing 3D surfaces from point clouds is a classic and important topic in computer graphics. The most widely used Poisson method [1, 22] fits surfaces by solving PDEs. These traditional methods involve adjusting the gradient of an indicator function to align with a solution derived from a (screened) Poisson equation. A crucial requirement of these methods is the input of oriented normals. The Iterative Screened Poisson Reconstruction method [23] introduced an iterative approach to refine the reconstruction process, improving the ability to generate surfaces from point clouds without direct computation of normals. The shape of points [24] introduced a differentiable point-to-mesh layer by employing a differentiable formulation of PSR [1] to generate watertight, topology-agnostic manifold surfaces.

Neural surface representations. Recently, the domain of deep learning has spurred significant advances in the implicit neural representation of 3D shapes. Some of these works trained a classifier neural network to construct occupancy fields [9, 10, 11, 12] for representing 3D geometries. Poco [12] achieves superior reconstruction performance by introducing convolution into occupancy fields. Ouasfi et al. [25] recently proposed a uncertainty measure method based on margin to learn occupancy fields from sparse point clouds. Compared to occupancy fields, SDFs [2, 3, 4, 5, 6, 7, 8] offer a more precise geometric representation by differentiating between interior and exterior spaces through the assignment of signs to distances. Some recent SOTA methods, such as DeepLS [3], using volumetric SDFs to locally learned continuous SDFs, have achieved higher compression, accuracy, and local shape refinement.

Unsigned distance fields learning. Although Occupancy fields and SDFs have undergone significant development recently, they are hard to reconstruct surfaces with boundaries or nonmanifold features. G-Shell [26] developed a differentiable shell-based representation for both watertight and non-watertight surfaces. However, UDFs provide a simpler and more natural way to represent general shapes [13, 14, 15, 16, 17, 18, 19, 20]. Various methods have

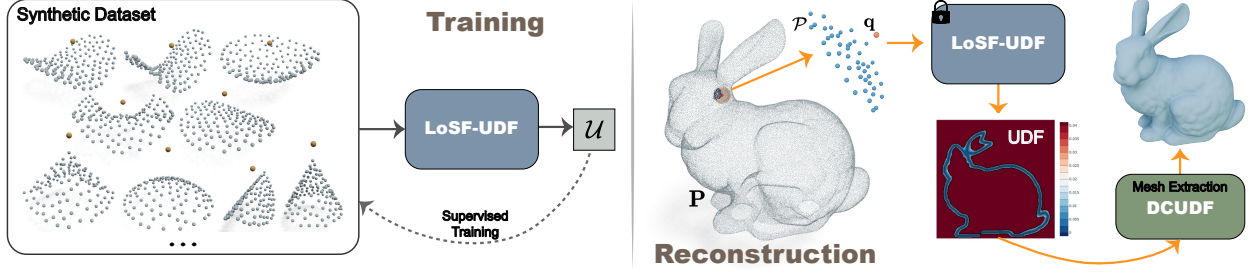


Figure 1: Pipeline. First, we train a UDF prediction network \mathcal{U}_Θ on a synthetic dataset, which contains a series of local point cloud patches that are independent of specific shapes. Given a global point cloud \mathbf{P} , we then extract a local patch \mathcal{P} assigned to each query point \mathbf{q} within a specified radius, and obtain the corresponding UDF values $\mathcal{U}_\Theta(\mathcal{P}, \mathbf{q})$. Finally, we extract the mesh corresponding to the input point cloud by incorporating the DCUDF[32] framework.

been proposed to reconstruct surfaces from point clouds by learning UDFs. CAP-UDF [17] suggested directing 3D query points towards the surface with a consistency constraint to develop UDFs that are aware of consistency. LevelSetUDF [14] learned a smooth zero-level function within UDFs through level set projections. As a supervised approach, GeoUDF [15] estimates UDFs by learning local geometric priors on many 3D shapes. DUDF [19] formulated the UDF learning as an Eikonal problem with distinct boundary conditions. UODF [20] proposed unsigned orthogonal distance fields that every point in this field can access to the closest surface points along three orthogonal directions. Instead of reconstructing from point clouds, many recent works [27, 28, 29, 30] learn high-quality UDFs from multi-view images for reconstructing non-watertight surfaces. Furthermore, UiDFF [31] presents a 3D diffusion model for UDFs to generate textured 3D shapes with boundaries.

3 Method

Motivation. Distinct from SDFs, there is no need for UDFs to determine the sign to distinguish between the inside and outside of a shape. Consequently, the UDF values are solely related to the local geometric characteristics of 3D shapes. Furthermore, within a certain radius for a query point, local geometry can be approximated by general mathematical functions. Stemming from these insights, we propose a novel UDF learning framework that focuses on local geometries. We employ local shape functions to construct a series of point cloud patches as our training dataset, which includes common smooth and sharp geometric features. Fig. 1 illustrates the pipeline of our proposed UDF learning framework.

3.1 Local shape functions

Smooth patches. From the viewpoint of differential geometry [33], the local geometry at a specific point on a regular surface can be approximated by a quadratic surface. Specifically, consider a regular surface $\mathcal{S} : \mathbf{r} = \mathbf{r}(u, v)$ with a point \mathbf{p} on it. At point \mathbf{p} , it is possible to identify two principal direction unit vectors, \mathbf{e}_1 and \mathbf{e}_2 , with the corresponding normal $\mathbf{n} = \mathbf{e}_1 \times \mathbf{e}_2$. A suitable parameter system (u, v) can be determined such that $\mathbf{r}_u = \mathbf{e}_1$ and $\mathbf{r}_v = \mathbf{e}_2$, thus obtaining the corresponding first and second fundamental forms as

$$[\text{I}]_{\mathbf{p}} = \begin{bmatrix} E & F \\ F & G \end{bmatrix} = \begin{bmatrix} 1 & 0 \\ 0 & 1 \end{bmatrix}, \quad [\text{II}]_{\mathbf{p}} = \begin{bmatrix} L & M \\ M & N \end{bmatrix} = \begin{bmatrix} \kappa_1 & 0 \\ 0 & \kappa_2 \end{bmatrix}, \quad (1)$$

where κ_1, κ_2 are principal curvatures. Without loss of generality, we assume \mathbf{p} corresponding to $u = v = 0$ and expand the Taylor form at this point as

$$\begin{aligned} \mathbf{r}(u, v) = & \mathbf{r}(0, 0) + \mathbf{r}_u(0, 0)u + \mathbf{r}_v(0, 0)v + \frac{1}{2}[\mathbf{r}_{uu}(0, 0)u^2 + \\ & \mathbf{r}_{uv}(0, 0)uv + \mathbf{r}_{vv}(0, 0)v^2] + o(u^2 + v^2). \end{aligned} \quad (2)$$

Decomposing $\mathbf{r}_{uu}(0, 0)$, $\mathbf{r}_{uv}(0, 0)$, and $\mathbf{r}_{vv}(0, 0)$ along the tangential and normal directions, we can formulate Eq.(2) according to Eq.(1) as

$$\begin{aligned} \mathbf{r}(u, v) = & \mathbf{r}(0, 0) + (u + o(\sqrt{u^2 + v^2}))\mathbf{e}_1 + (v + o(\sqrt{u^2 + v^2}))\mathbf{e}_2 \\ & + \frac{1}{2}(\kappa_1 u^2 + \kappa_2 v^2 + o(u^2 + v^2))\mathbf{n} \end{aligned} \quad (3)$$

where $o(u^2 + v^2) \approx 0$ is negligible in a small local region. Consequently, by adopting $\{\mathbf{p}, \mathbf{e}_1, \mathbf{e}_2, \mathbf{n}\}$ as the orthogonal coordinate system, we can define the form of the local approximating surface as

$$x = u, \quad y = v, \quad z = \frac{1}{2}(\kappa_1 u^2 + \kappa_2 v^2), \quad (4)$$

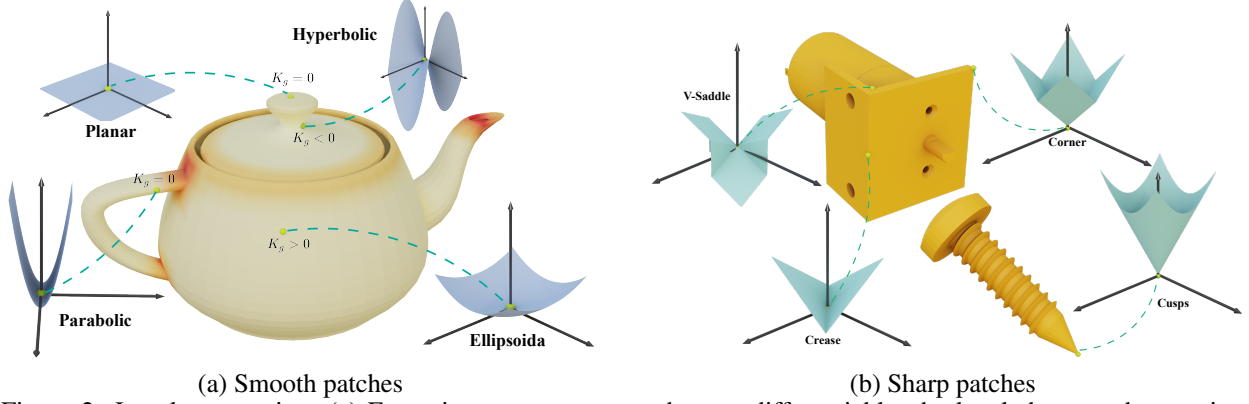


Figure 2: Local geometries. (a) For points on a geometry that are differentiable, the local shape at these points can be approximated by quadratic surfaces. (b) For points that are non-differentiable, we can also construct locally approximated surfaces using functions.

which exactly are quadratic surfaces $z = \frac{1}{2}(\kappa_1 x^2 + \kappa_2 y^2)$. Furthermore, in relation to Gaussian curvatures $\kappa_1 \kappa_2$, quadratic surfaces can be categorized into four types: ellipsoidal, hyperbolic, parabolic, and planar. As shown in Fig. 2, for differentiable points on a general geometry, the local shape features can always be described by one of these four types of quadratic surfaces.

Sharp patches. For surfaces with sharp features, they are not differentiable at some points and cannot be approximated in the form of a quadratic surface. We categorize commonly seen sharp geometric features into four types, including creases, cusps, corners, and v-saddles, as illustrated in Fig. 2(b). We construct these four types of sharp features in a consistent form $z = f(x, y)$ like smooth patches

$$\begin{aligned} \text{creases: } z &= 1 - h \cdot \frac{|kx - y|}{\sqrt{1 + k^2}}, & \text{cusps: } z &= 1 - h \cdot \sqrt{x^2 + y^2}, \\ \text{corners: } z &= 1 - h \cdot \max(|x|, |y|), & \text{v-saddles: } z &= 1 - h \cdot |x| + |y| \cdot \left(\frac{|x|}{x} \cdot \frac{|y|}{y}\right), \end{aligned} \quad (5)$$

where h can adjust the sharpness of the shape, and k can control the direction of the crease. Fig 3 illustrates various smooth and sharp patches with distinct parameters.

Synthetic training dataset. We utilize the mathematical functions introduced above to synthesize a series of point cloud patches for training. As shown in Fig. 3, we first uniformly sample m points $\{(x_i, y_i)\}_{i=1}^m$ within a circle of radius r_0 centered at $(0, 0)$ in the xy -plane. Then, we substitute the coordinates into Eq.(4-5) to obtain the corresponding z -coordinate values, resulting in a patch $\mathcal{P} = \{\mathbf{p}_i\}_{i=1}^m$, where $\mathbf{p}_i = (x_i, y_i, z(x_i, y_i))$. Subsequently, we randomly collect query points $\{\mathbf{q}_i\}_{i=1}^n$ distributed along the vertical ray intersecting the xy -plane at the origin, extending up to a distance of r_0 . For each query point \mathbf{q}_i , we determine its UDF value $\mathcal{U}(\mathbf{q}_i)$, which is either $|\mathbf{q}_i^{(z)}|$ for smooth patches or $1 - |\mathbf{q}_i^{(z)}|$ for sharp patches. Noting that for patches with excessively high curvature or sharpness, the minimum distance of the query points may not be the distance to $(0, 0, z(0, 0))$, we will exclude these patches from our training dataset. Overall, each sample in our synthetic dataset is specifically in the form of $\{\mathbf{q}, \mathcal{P}, \mathcal{U}(\mathbf{q})\}$.

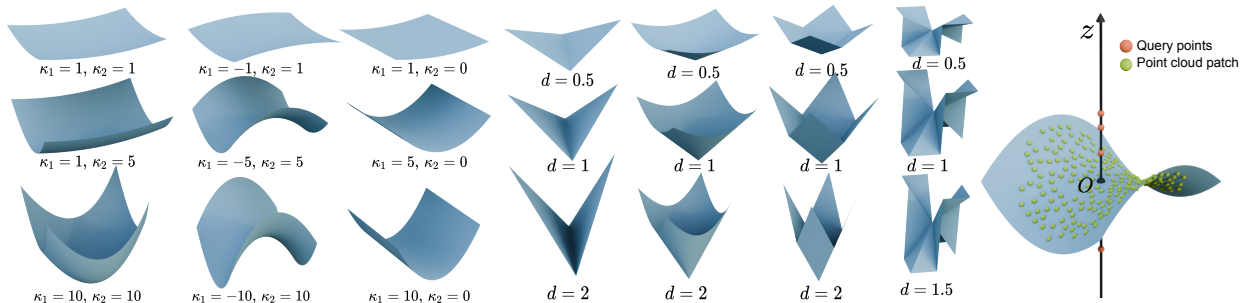


Figure 3: Synthetic dataset for training. By manipulating functional parameters, we can readily create various smooth and sharp surfaces, subsequently acquiring pairs of point cloud patches and query points via sampling.

3.2 UDF learning

We perform supervised training on the synthesized dataset which is independent of specific shapes. The network learns the features of local geometries and utilizes an attention-based module to output the corresponding UDF values from the learned features. After training, given any 3D point clouds and a query point in space, we extract the local point cloud patch near the query, which has the same form as the data in the training dataset. Consequently, our network can predict the UDF value at that query point based on this local point cloud patch.

3.2.1 Network architecture

For a sample $\{\mathbf{q}, \mathcal{P} = \{\mathbf{p}_i\}_{i=1}^m, \mathcal{U}(\mathbf{q})\}$, we first obtain a latent code $\mathbf{f}_p \in \mathbb{R}^{l_p}$ related to the local point cloud patch \mathcal{P} through a Point-Net [34] \mathcal{F}_p . To derive features related to distance, we use relative vectors from the patch points to the query point, $\mathcal{V} = \{\mathbf{p}_i - \mathbf{q}\}_{i=1}^m$, as input to a Vectors-Net \mathcal{F}_v , which is similar to the Point-Net \mathcal{F}_p . This process results in an additional latent code $\mathbf{f}_v \in \mathbb{R}^{l_v}$. Subsequently, we apply a cross-attention module [35] to obtain the feature codes for the local geometry,

$$\mathbf{f}_G = \text{CrossAttn}(\mathbf{f}_p, \mathbf{f}_v) \in \mathbb{R}^{l_G}, \quad (6)$$

where we take \mathbf{f}_p as the Key-Value (KV) pair and \mathbf{f}_v as the Query (Q). In our experiments, we set $l_p = l_v = 64$, and $l_G = 128$. Based on the learned geometric features, we aim to fit the UDF values from the distance within the local point cloud. Therefore, we concatenate the distances $\mathbf{d} \in \mathbb{R}^m$ induced from \mathcal{V} with the latent code \mathbf{f}_G , followed by a series of fully connected layers to output the predicted UDF values $\mathcal{U}_\Theta(\mathbf{q})$. Fig. 4 illustrates the overall network architecture and data flow. The two PointNets used in our network to extract features from point cloud patches \mathcal{P} and vectors \mathcal{V} consist of four ResNet blocks. In addition, the two fully connected layer modules in our framework consist of three layers each. To ensure non-negativity of the UDF values output by the network, we employ the softplus activation function.

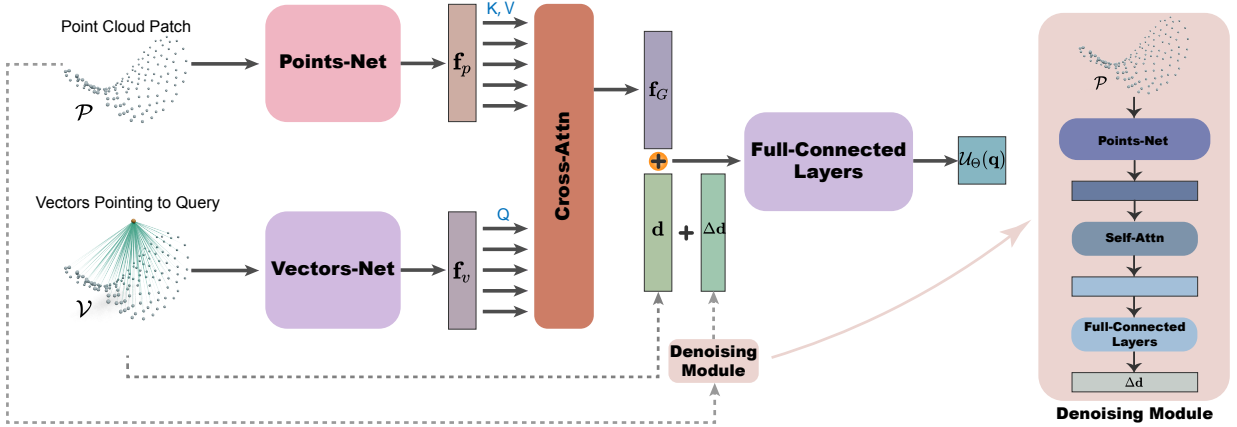


Figure 4: Network architecture of LoSF-UDF.

Denoising module. In our network, even if point cloud patches are subjected to a certain degree of noise or outliers, their representations in the feature space should remain similar. However, distances induced directly from noisy vectors \mathcal{V} will inevitably contain errors, which can affect the accurate prediction of UDF values. To mitigate this impact, we introduce a denoising module that predicts displacements $\Delta \mathbf{d}$ from local point cloud patches, as shown in Fig. 4. We then add the displacements $\Delta \mathbf{d}$ to the distances \mathbf{d} to improve the accuracy of the UDF estimation.

3.2.2 Training and evaluation

Data augmentation. During the training process, we scale all pairs of local patches \mathcal{P} and query points \mathbf{q} to conform to the bounding box constraints of $[-0.5, 0.5]$, and the corresponding GT UDF values $\mathcal{U}(\mathbf{q})$ are scaled by equivalent magnitudes. Given the uncertain orientation of local patches extracted from a specified global point cloud, we have applied data augmentation via random rotations to the training dataset. Furthermore, to enhance generalization to open surfaces with boundaries, we randomly truncate 20% of the smooth patches to simulate boundary cases. To address the issue of noise handling, we introduce Gaussian noise $\mathcal{N}(0, 0.1)$ to 30% of the data in each batch during every training epoch.

Loss functions. We employ L_1 loss \mathcal{L}_u to measure the discrepancy between the predicted UDF values and the GT UDF values. Moreover, for the displacements $\Delta \mathbf{d}$ output by the denoising module, we employ L_1 regularization to

encourage sparsity. Consequently, we train the network driven by the following loss function,

$$\mathcal{L} = \mathcal{L}_u + \lambda_d \mathcal{L}_r, \quad \text{where } \mathcal{L}_u = |\mathcal{U}(\mathbf{q}) - \mathcal{U}_\Theta(\mathbf{q})|, \quad \mathcal{L}_r = |\Delta \mathbf{d}|, \quad (7)$$

where we set $\lambda_d = 0.01$ in our experiments.

Evaluation. Given a 3D point cloud \mathbf{P} for reconstruction, we first normalize it to fit within a bounding box with dimensions ranging from $[-0.5, 0.5]$. Subsequently, within the bounding box space, we uniformly sample grid points at a specified resolution to serve as query points. Finally, we extract the local geometry \mathcal{P}_p for each query point by collecting points from the point cloud that lie within a sphere of a specified radius centered on the query point. We can obtain the predicted UDF values by the trained network $\mathcal{U}_{\Theta^*}(\mathbf{q}, \mathcal{P}_p)$, where Θ^* represents the optimized network parameters. Note that for patches \mathcal{P}_p with fewer than 5 points, we set the UDF values as a large constant. Finally, we extract meshes from the UDFs using the DCUDF model [32].

4 Experiments

4.1 Experiment setup

Datasets. To compare our method with other state-of-the-art UDF learning approaches, we tested it on various datasets that include general artificial objects from the field of computer graphic. Following previous works [30, 17, 14], we select the "Car" category from ShapeNet[21], which has a rich collection of multi-layered and non-closed shapes. Furthermore, we select the real-world dataset DeepFashion3D[36] for open surfaces, and ScanNet[37] for large outdoor scenes. To assess our model’s performance on actual noisy inputs, we conducted tests on real range scan dataset [38] following the previous works[17, 14].

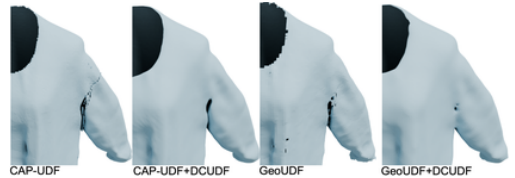
Baselines. For our validation datasets, we compared our method against the state-of-the-art UDF learning models, which include unsupervised methods like CAP-UDF[17], LevelSetUDF[14], and DUDF[19], as well as the supervised learning method, GeoUDF[15]. We trained GeoUDF independently on different datasets to achieve optimal performance. Table. 1 shows the qualitative comparison between our methods and baselines. To evaluate performance, we calculate the Chamfer Distance (CD) and F1-Score (setting thresholds of 0.005 and 0.01) metrics between the ground truth meshes and the meshes extracted from the UDFs out by our model and each baseline model. For a fair comparison, we test all baseline models using the DCUDF[32] method. All experimental procedures are executed on NVIDIA RTX 4090 and A100 GPUs.

Methods	Input	Normal	Learning Type	Feature Type	Noise	Outlier
CAP-UDF [17]	Dense	Not required	Unsupervised	Global	✗	✗
LevelSetUDF [14]	Dense	Not required	Unsupervised	Global	✓	✗
GeoUDF [15]	Sparse	Not required	Supervised	Local	✗	✗
DUDF [19]	Dense	Required	Unsupervised	Global	✗	✗
Ours	Dense	Not required	Supervised	Local	✓	✓

Table 1: Qualitative comparison of different UDF learning methods. “Normal” indicates whether the method requires point cloud normals during learning. “Feature Type” refers to whether the information required during training is global or local. “Noise” and “Outlier” indicate whether the method can handle the presence of noise and outliers in point clouds.

4.2 Experimental results

Synthetic data. For general 3D graphic models, ShapeNetCars, and DeepFashion3D, we obtain dense point clouds by randomly sampling on meshes. Considering that GeoUDF [15] is a supervised method, we retrain it on ShapeNetCars, and DeepFashion3D, which are randomly partitioned into training (70%), testing (20%), and validation subsets (10%). All models are evaluated in the validation sets, which remain unseen by any of the UDF learning models prior to evaluation. The first three rows of Fig. 5 show the visual comparison of reconstruction results, while Tab. 2 presents the quantitative comparison results of CD and F1-score. We test each method using their own mesh extraction technique, as shown in the inset figure, which display obvious visual artifacts such as small holes and non-smoothness. We thus apply DCUDF [32], the state-of-art method, to each baseline model, extracting the surfaces as significantly higher quality meshes. Since our method utilizes DCUDF for surface extraction, we adopt it as the default technique to ensure consistency and fairness in comparisons with the baselines. Our method achieves stable



results in reconstructing various types of surfaces, including both open and closed surfaces, and exhibits performance comparable to that of the SOTA methods. Noting that DUDF [19] requires normals during training, and GeoUDF utilizes the KNN approach to determine the nearest neighbors of the query points. Although DUDF and GeoUDF achieve better evaluations, they are less stable when dealing with point clouds with noise and outliers.

		Clean			Noise			Outlier		
		CD ↓	F1 ↑		CD ↓	F1 ↑		CD ↓	F1 ↑	
method			$F1^{0.005}$	$F1^{0.01}$		$F1^{0.005}$	$F1^{0.01}$		$F1^{0.005}$	$F1^{0.01}$
ShapeNetCars [21]	CAP-UDF [17]	2.432	0.523	0.888	2.602	0.194	0.381	4.982	0.183	0.314
	LevelSetUDF [14]	1.534	0.561	0.908	2.490	0.209	0.401	4.177	0.199	0.363
	GeoUDF [15]	1.257	0.571	0.889	1.232	0.351	0.873	4.870	0.187	0.346
	DUDF [19]	0.568	0.903	0.991	3.180	0.312	0.527	4.235	0.168	0.308
	Ours	1.085	0.510	0.938	1.114	0.427	0.922	1.272	0.485	0.771
DeepFashion3D [36]	CAP-UDF [17]	1.660	0.417	0.818	1.892	0.336	0.542	4.941	0.172	0.430
	LevelSetUDF [14]	1.500	0.403	0.856	1.488	0.453	0.729	4.328	0.203	0.468
	GeoUDF [15]	0.652	0.864	0.977	1.258	0.380	0.957	4.463	0.147	0.300
	DUDF [19]	0.381	0.991	0.998	1.894	0.334	0.535	4.970	0.144	0.272
	Ours	0.932	0.652	0.983	1.150	0.361	0.976	1.029	0.549	0.973

Table 2: Quantitative evaluation of UDF learning methods (CD score is multiplied by 100).

Noise & outliers. To evaluate our model with noisy inputs, we added Gaussian noise $\mathcal{N}(0, 0.0025)$ to the clean data across all datasets for testing. The middle three rows in Fig. 5 display the reconstructed surface results from noisy point clouds, and Tab. 2 also presents the quantitative comparisons. It can be observed that our method can robustly reconstruct smooth surfaces from noisy point clouds. Additionally, we tested our method’s performance with outliers by converting 10% of the clean point cloud into outliers, as shown in the last three rows of Fig. 5. To further demonstrate the robustness of our method, we conducted experiments on point clouds with higher percentage of outliers. Our framework is able of reconstructing reasonable surfaces even with 50% outliers, as shown in Fig. 6. Furthermore, our approach can reconstruct high-quality geometry from point clouds containing both noise and outliers.

Real-world scanned data. Dataset [38] provide several real-world scanned point clouds, as illustrated in Fig. 7 (Left), we evaluate our model on the dataset to demonstrate the effectiveness. Our approach can reconstruct smooth surfaces from scanned data containing noise and outliers. However, our model cannot address the issue of missing parts. This limitation is due to the local geometric training strategy, which is independent of the global shape. Additionally, we conduct tests on large scanned scenes to evaluate our algorithm, as shown in Fig. 7 (Right).

4.3 Analysis & ablation studies

Efficiency. As a supervised UDF learning method, our approach has a significant improvement in training efficiency compared to GeoUDF [15]. As shown in the insert table, we calculate the data storage space required by GeoUDF when using ShapeNet as a training dataset. This includes the GT UDF values and point cloud data needed during the training process. Our synthetic point cloud patches training dataset occupies under 1GB, which is merely 0.5% of the storage needed for GeoUDF. Our network is very lightweight, with only 653KB of trainable parameters and a total parameter size of just 2MB. Additionally, we highlight time-saving benefits. The provided table illustrates the duration required to produce a single data sample for dataset preparation (“Data-prep”), as well as the total time for training (“Training”).

Method	Storage (GB)	Data-prep (min)	Training (h)
GeoUDF	120	0.5	36
Ours	0.59	0.02	14.5

Patch radius. During the evaluation phase, the radius r used to find the nearest points for each query point determines the size of the extracted patch and the range of effective query points in the space. As shown in Fig. 8, we analyzed the impact of different radii on the reconstruction results. An excessively small r will generate artifacts, while an overly large r will lose many details. In our experiments, we generally set r to 0.018.

Denosing module. Our framework incorporates a denosing module to handle noisy point clouds. We conducted ablation experiments to verify the significance of this module. Specifically, we set $\lambda_d = 0$ in the loss function Eq. (7) to disable the denosing module, and then retrained the network. As illustrated in Fig. 9, we present the reconstructed surfaces for the same set of noisy point clouds with and without the denosing module, respectively.

5 Conclusion

In this paper, we introduce a novel and efficient neural framework for surface reconstruction from 3D point clouds by learning UDFs from local shape functions. Our key insight is that 3D shapes exhibit simple patterns within localized regions, which can be exploited to create a training dataset of point cloud patches represented by mathematical functions.

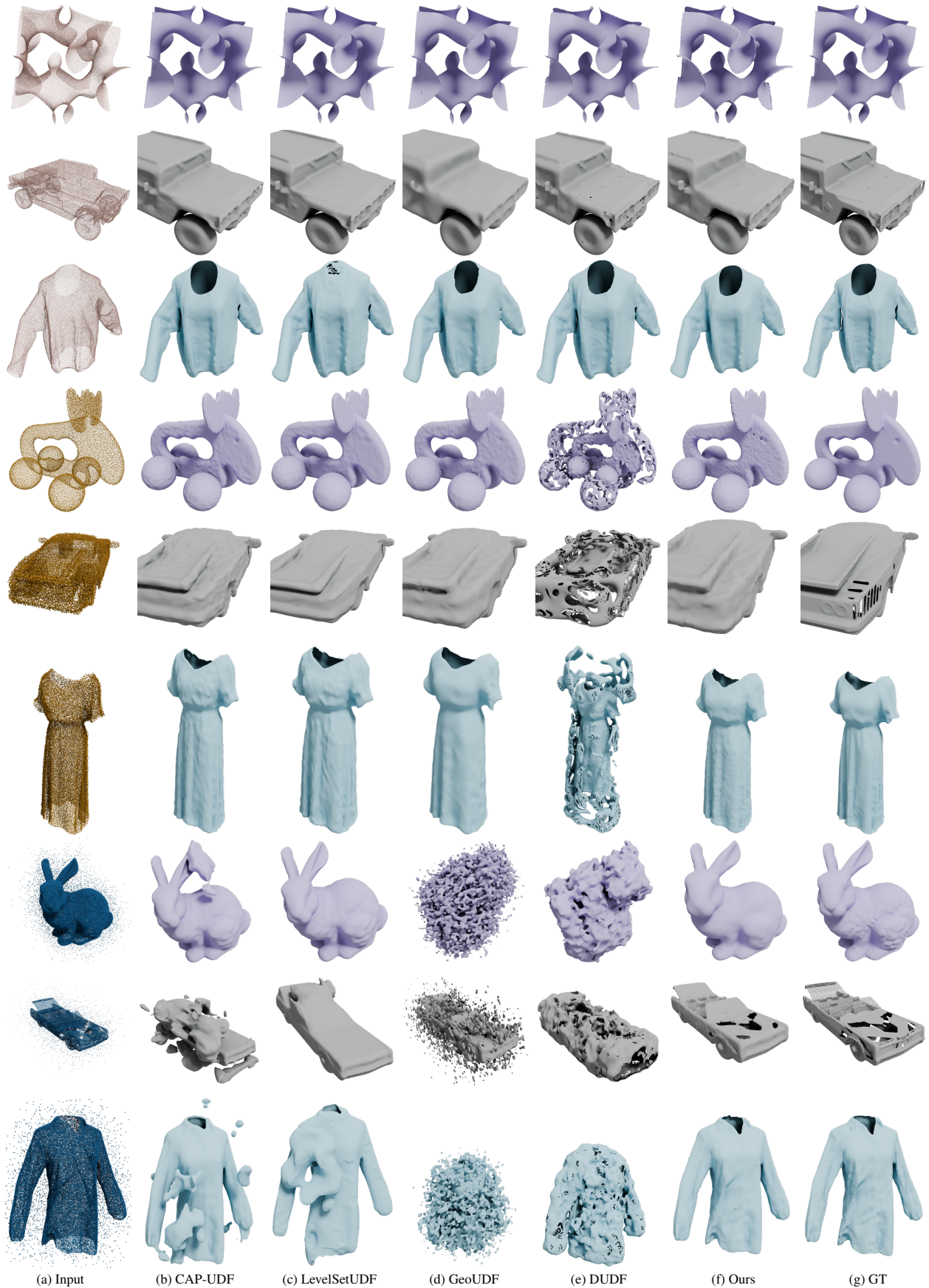


Figure 5: Visual comparisons on the synthetic dataset. First three rows: uniformly sampled points. Middle three rows: point clouds with 0.25% added noise. Last three rows: point clouds with 10% outliers. All point clouds here have 48K points, except for the Bunny model, which has 100K points. We refer readers to the appendix for more visual results.

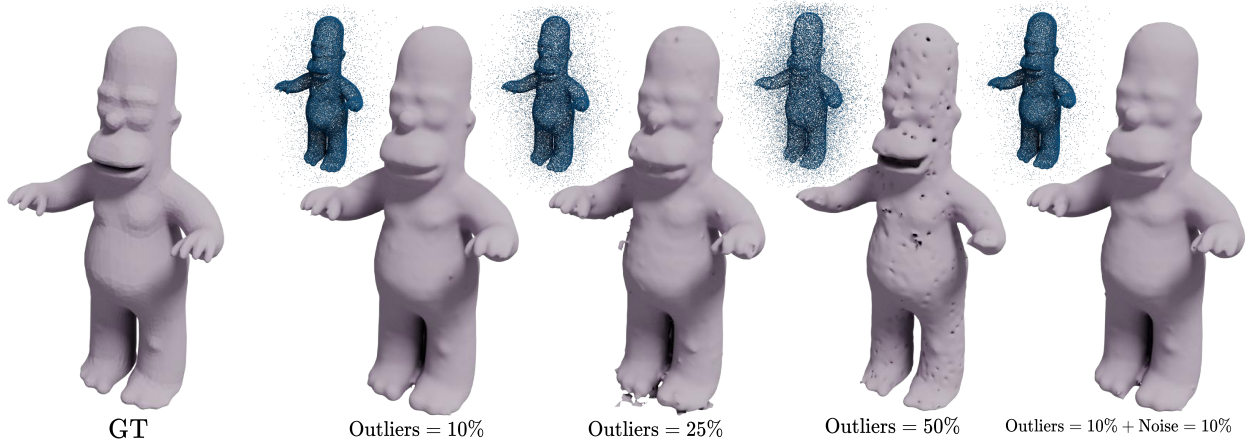


Figure 6: Our model demonstrates robustness to more outliers.



Figure 7: Reconstructed surfaces from real-world scanned point clouds.



Figure 8: Comparison of different radii for extracting patches from the point cloud on reconstruction results.

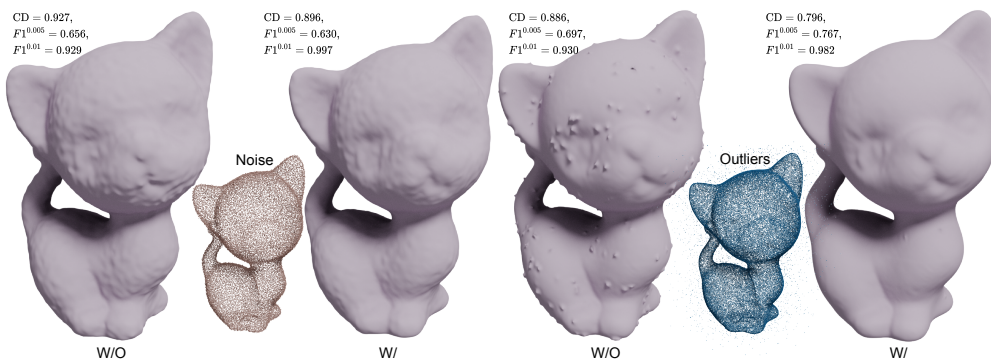


Figure 9: Ablation on denoising module: Reconstructed surfaces from the same point clouds with noise/outliers corresponding to framework with and without the denoising module, respectively.

As a result, our method enables efficient and robust surfaces reconstructions without the need for shape-specific training. Extensive experiments on various datasets have demonstrated the efficacy of our method. Moreover, our framework achieves superior performance on point clouds with noise and outliers.

Limitations & future work. Owing to its dependence solely on local geometric features, our approach fails to address tasks involving incomplete point cloud reconstructions. However, as a lightweight framework, our model can readily be integrated into other unsupervised methods to combine the global features with our learned local priors. Furthermore, in our future work, we intend to design a method that dynamically adjusts the radius based on local feature sizes [39] of 3D shapes when extracting local point cloud patches for queries, aiming to improve the accuracy of the reconstruction.

References

- [1] M Kazhdan. Poisson surface reconstruction. In *Eurographics Symposium on Geometry Processing*, 2006.
- [2] Jeong Joon Park, Peter Florence, Julian Straub, Richard Newcombe, and Steven Lovegrove. Deep sdf: Learning continuous signed distance functions for shape representation. In *The IEEE Conference on Computer Vision and Pattern Recognition (CVPR)*, June 2019.
- [3] Rohan Chabra, Jan Eric Lenssen, Eddy Ilg, Tanner Schmidt, Julian Straub, Steven Lovegrove, and Richard Newcombe. Deep local shapes: Learning local sdf priors for detailed 3d reconstruction, 2020.
- [4] Ma Baorui, Han Zhizhong, Liu Yu-Shen, and Zwicker Matthias. Neural-pull: Learning signed distance functions from point clouds by learning to pull space onto surfaces. In *International Conference on Machine Learning (ICML)*, 2021.
- [5] Peng-Shuai Wang, Yang Liu, and Xin Tong. Dual octree graph networks for learning adaptive volumetric shape representations. *ACM Transactions on Graphics*, 41(4):1–15, July 2022.
- [6] Liu Shi-Lin, Guo Hao-Xiang, Pan Hao, Peng-Shuai Wang, Tong Xin, and Liu Yang. Deep implicit moving least-squares functions for 3d reconstruction. In *IEEE/CVF Conference on Computer Vision and Pattern Recognition*, 2021.
- [7] Zixiong Wang, Pengfei Wang, Pengshuai Wang, Qiuji Dong, Junjie Gao, Shuangmin Chen, Shiqing Xin, Changhe Tu, and Wenping Wang. Neural-impls: Self-supervised implicit moving least-squares network for surface reconstruction. *IEEE Transactions on Visualization and Computer Graphics*, pages 1–16, 2023.
- [8] Ma Baorui, Liu Yu-Shen, and Han Zhizhong. Reconstructing surfaces for sparse point clouds with on-surface priors. In *Proceedings of the IEEE/CVF Conference on Computer Vision and Pattern Recognition (CVPR)*, 2022.
- [9] Lars Mescheder, Michael Oechsle, Michael Niemeyer, Sebastian Nowozin, and Andreas Geiger. Occupancy networks: Learning 3d reconstruction in function space. In *Proceedings IEEE Conf. on Computer Vision and Pattern Recognition (CVPR)*, 2019.
- [10] Julian Chibane, Thiemo Alldieck, and Gerard Pons-Moll. Implicit functions in feature space for 3d shape reconstruction and completion. In *IEEE Conference on Computer Vision and Pattern Recognition (CVPR)*. IEEE, jun 2020.
- [11] Songyou Peng, Michael Niemeyer, Lars Mescheder, Marc Pollefeys, and Andreas Geiger. Convolutional occupancy networks. In *European Conference on Computer Vision (ECCV)*, 2020.
- [12] Alexandre Boulch and Renaud Marlet. Poco: Point convolution for surface reconstruction, 2022.
- [13] Julian Chibane, Aymen Mir, and Gerard Pons-Moll. Neural unsigned distance fields for implicit function learning. In *Advances in Neural Information Processing Systems (NeurIPS)*, December 2020.
- [14] Junsheng Zhou, Baorui Ma, Shujuan Li, Yu-Shen Liu, and Zhizhong Han. Learning a more continuous zero level set in unsigned distance fields through level set projection. In *Proceedings of the IEEE/CVF international conference on computer vision*, 2023.
- [15] Siyu Ren, Junhui Hou, Xiaodong Chen, Ying He, and Wenping Wang. Geoudf: Surface reconstruction from 3d point clouds via geometry-guided distance representation. In *Proceedings of the IEEE/CVF International Conference on Computer Vision*, pages 14214–14224, 2023.
- [16] Jianglong Ye, Yuntao Chen, Naiyan Wang, and Xiaolong Wang. Gifs: Neural implicit function for general shape representation. In *Proceedings of the IEEE/CVF Conference on Computer Vision and Pattern Recognition*, 2022.
- [17] Junsheng Zhou, Baorui Ma, Yu-Shen Liu, Yi Fang, and Zhizhong Han. Learning consistency-aware unsigned distance functions progressively from raw point clouds. In *Advances in Neural Information Processing Systems (NeurIPS)*, 2022.
- [18] Qing Li, Huifang Feng, Kanle Shi, Yi Fang, Yu-Shen Liu, and Zhizhong Han. Neural gradient learning and optimization for oriented point normal estimation. In *SIGGRAPH Asia 2023 Conference Papers*, 2023.
- [19] Miguel Fainstein, Viviana Siless, and Emmanuel Iarussi. Duf: Differentiable unsigned distance fields with hyperbolic scaling, 2024.
- [20] Yujie Lu, Long Wan, Nayu Ding, Yulong Wang, Shuhan Shen, Shen Cai, and Lin Gao. Unsigned orthogonal distance fields: An accurate neural implicit representation for diverse 3d shapes. In *IEEE/CVF Conference on Computer Vision and Pattern Recognition (CVPR)*, 2024.

- [21] Angel X. Chang, Thomas Funkhouser, Leonidas Guibas, Pat Hanrahan, Qixing Huang, Zimo Li, Silvio Savarese, Manolis Savva, Shuran Song, Hao Su, Jianxiong Xiao, Li Yi, and Fisher Yu. ShapeNet: An Information-Rich 3D Model Repository. Technical Report arXiv:1512.03012 [cs.GR], Stanford University — Princeton University — Toyota Technological Institute at Chicago, 2015.
- [22] Michael Kazhdan and Hugues Hoppe. Screened poisson surface reconstruction. *Acm Transactions on Graphics*, 32(3):1–13, 2013.
- [23] Fei Hou, Chiyu Wang, Wencheng Wang, Hong Qin, Chen Qian, and Ying He. Iterative poisson surface reconstruction (ipsr) for unoriented points. *ACM Transactions on Graphics*, 41(4):1–13, July 2022.
- [24] Songyou Peng, Chiyu "Max" Jiang, Yiyi Liao, Michael Niemeyer, Marc Pollefeys, and Andreas Geiger. Shape as points: A differentiable poisson solver. In *Advances in Neural Information Processing Systems (NeurIPS)*, 2021.
- [25] Amine Ouasfi and Adnane Boukhayma. Unsupervised occupancy learning from sparse point cloud, 2024.
- [26] Zhen Liu, Yao Feng, Yuliang Xiu, Weiyang Liu, Liam Paull, Michael J. Black, and Bernhard Schölkopf. Ghost on the shell: An expressive representation of general 3d shapes. 2024.
- [27] Junkai Deng, Fei Hou, Xuhui Chen, Wencheng Wang, and Ying He. 2s-udf: A novel two-stage udf learning method for robust non-watertight model reconstruction from multi-view images, 2024.
- [28] Xiaoxu Meng, Weikai Chen, and Bo Yang. Neat: Learning neural implicit surfaces with arbitrary topologies from multi-view images. *Proceedings of the IEEE/CVF Conference on Computer Vision and Pattern Recognition*, June 2023.
- [29] Xiaoxiao Long, Cheng Lin, Lingjie Liu, Yuan Liu, Peng Wang, Christian Theobalt, Taku Komura, and Wenping Wang. Neuraludf: Learning unsigned distance fields for multi-view reconstruction of surfaces with arbitrary topologies. In *Proceedings of the IEEE/CVF Conference on Computer Vision and Pattern Recognition*, pages 20834–20843, 2023.
- [30] Yu-Tao Liu, Li Wang, Jie Yang, Weikai Chen, Xiaoxu Meng, Bo Yang, and Lin Gao. Neudf: Leaning neural unsigned distance fields with volume rendering. In *Computer Vision and Pattern Recognition (CVPR)*, 2023.
- [31] Junsheng Zhou, Weiqi Zhang, Baorui Ma, Kanle Shi, Yu-Shen Liu, and Zhizhong Han. Udiff: Generating conditional unsigned distance fields with optimal wavelet diffusion. In *Proceedings of the IEEE/CVF Conference on Computer Vision and Pattern Recognition*, 2024.
- [32] Fei Hou, Xuhui Chen, Wencheng Wang, Hong Qin, and Ying He. Robust zero level-set extraction from unsigned distance fields based on double covering. *ACM Trans. Graph.*, 42(6), dec 2023.
- [33] Manfredo P Do Carmo. *Differential geometry of curves and surfaces: revised and updated second edition*. Courier Dover Publications, 2016.
- [34] Charles Ruizhongtai Qi, Li Yi, Hao Su, and Leonidas J Guibas. Pointnet++: Deep hierarchical feature learning on point sets in a metric space. *Advances in neural information processing systems*, 30, 2017.
- [35] Ashish Vaswani, Noam Shazeer, Niki Parmar, Jakob Uszkoreit, Llion Jones, Aidan N. Gomez, Lukasz Kaiser, and Illia Polosukhin. Attention is all you need, 2023.
- [36] Ziwei Liu, Ping Luo, Shi Qiu, Xiaogang Wang, and Xiaoou Tang. Deepfashion: Powering robust clothes recognition and retrieval with rich annotations. In *Proceedings of IEEE Conference on Computer Vision and Pattern Recognition (CVPR)*, June 2016.
- [37] Angela Dai, Angel X. Chang, Manolis Savva, Maciej Halber, Thomas Funkhouser, and Matthias Nießner. Scannet: Richly-annotated 3d reconstructions of indoor scenes. In *Proc. Computer Vision and Pattern Recognition (CVPR), IEEE*, 2017.
- [38] Matthew Berger, Joshua A. Levine, Luis Gustavo Nonato, Gabriel Taubin, and Claudio T. Silva. A benchmark for surface reconstruction. *ACM Trans. Graph.*, 32(2), apr 2013.
- [39] Yulan Guo, Mohammed Bannamoun, Ferdous Sohel, Min Lu, Jianwei Wan, and Ngai Ming Kwok. A comprehensive performance evaluation of 3d local feature descriptors. *International Journal of Computer Vision*, 116:66–89, 2016.

A Appendix

A.1 More results

As shown in Fig. 10 and Fig. 11, we provide more visual comparisons on the DeepFashion3D and ShapeNetCars dataset, using point clouds containing noise and outliers.



Figure 10: More visual results on the DeepFashion3D dataset. Top three rows: Reconstruction results under noise-free conditions. Bottom three rows: Reconstruction results under noise condition.

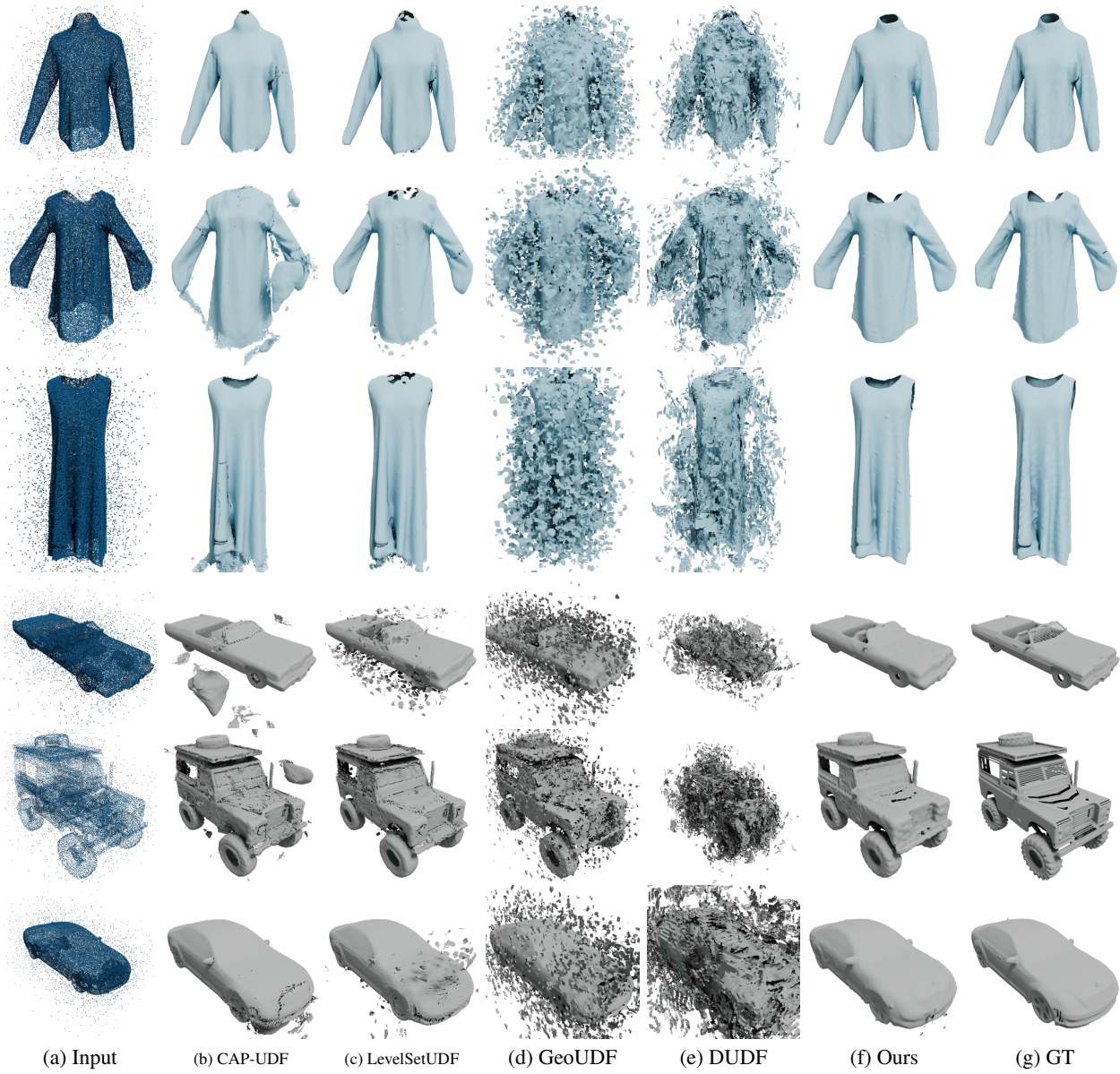


Figure 11: More visual results on the synthetic datasets with outliers.